Appendices

1 The latent zoospore pool transmission model

Using the mesocosm transmission experiment described in the main text, we sought to characterize the transmission function for Bd and *R. muscosa*. In particular, we wanted to quantify how the environmental zoospore pool affected the probability of an amphibian transitioning from infected to uninfected in a time step. However, we were unable to measure the total number of zoospores in the environmental zoospore pool at each time step and therefore assumed that the zoospore pool was a latent variable that needed to be estimated. We estimated it by assuming that the zoospore pool obeyed the following dynamics

$$Z_j(t+\Delta t) = Z_j(t)\exp(-d^*\Delta t) + Z_{j,\text{tadpoles}}(t)f_T^*\Delta t + Z_{j,\text{adults}}(t)f_A^*\Delta t \tag{1}$$

This equation assumes that the dynamics of the unobserved zoospore pool in mesocosm j are governed by the survival probability of zoospores in the pool at time t (first term, d^* is zoospore death rate) and contribution of zoospores into the pool based on the total number of zoospores on tadpoles ($Z_{j,\text{tadpoles}}(t)$) and adults ($Z_{j,\text{adults}}(t)$) at time t in mesocosm j. f_T^* and f_A^* are rates that relate the total number of zoospores on tadpoles and frogs at time t (as estimated from qPCR) to the total number of zoospores that enter the pool. This equation does not include the reduction of zoospores in the pool due to frogs acquiring them upon initial infection as we found that the small number acquired is inconsequential for the dynamics of the zoospore pool.

For the ith individual frog in mesocosm j at time $t+1$, the likelihood of gaining an infection is given by

$$y_{ij}(t+\Delta t) \sim \text{Bernoulli}(\phi_j(t)) \text{ if } y_{ij}(t) = 0 \tag{2}$$

Each individual frog i in tank j was swabbed six times over the course of 32 days and $y_{ij}(t)$ specifies whether frog i in mesocosm j was infected (1) or uninfected (0) at time $t+\Delta t$, having been uninfected at time t. Only observations where an animal was uninfected in the previous time step directly contributed to the likelihood ($n = 333$), but the entire time series for all individuals within a mesocosm contributed to the dynamics of the zoospore pool.

$\phi_j(t)$ is the probability of infection in mesocosm j at time t and takes the general functional form

$$\phi_j(t) = 1 - \exp(-\Lambda(Z_j(t), A_j(t), I_j(t))\Delta t) \tag{3}$$

where the probability of infection depends on the total number of zoospores in the pool ($Z_j(t)$), the total number of adults ($A_j(t)$), and the total number of infecteds ($I_j(t)$) in tank j at time t. The number of adults and total number of infecteds are both observed (i.e. measured in the experiment) at each time t. In contrast, $Z_j(t)$ is unobserved at each time t. The specific forms of $\Lambda(Z_j(t), A_j(t), I_j(t))$ that we considered are given in Table 2 in the main text.

We assumed that the total number of zoospores $Z_j(t)$ is a random variable with a lognormal distribution such that

$$\ln(Z_j(t + \Delta t)) \sim \text{Normal}(\ln(\mu_j(t + \Delta t)) - \frac{\sigma^2}{2}), \sigma^2) \tag{4}$$

$$\mu_j(t + \Delta t) = Z(t)_j \exp(-d^* \Delta t) + Z_{\text{tadpoles}}(t)_j f_T^* \Delta t + Z_{\text{adults}}(t)_j f_A^* \Delta t \tag{5}$$

$Z_{\text{tadpoles}}(t)_j$ and $Z_{\text{adults}}(t)_j$ were both observed at each time t. The $\frac{\sigma^2}{2}$ terms is a result of converting from the expected value of the lognormal distribution to the mean of the normal distribution on the log scale.

To fit these models, we assumed that the initial zoospore load in the pool was given by $\ln Z_j(t = 0) \sim \text{Normal}(\ln(2000), \sigma^2)$. We specified this prior distribution based on the average number zoospores on the tadpoles at the beginning of the experiment across all mesocosms. We gave the zoospore death rate d^* day^{-1} a normal prior distribution with mean 0.3 day^{-1}, standard deviation 0.03, and a lower bound of 0. This tight prior was based on laboratory estimates of the zoospore death rate (Woodhams *et al.* 2008). To aid in the identifiability of our model, we set $\sigma = 1$ and $f_T = f_A = f$ and gave f a vague half Cauchy prior distribution with a scale parameter equal to 1.

We fit this model for each of the ϕ functions given in Table 2 in the main text using Hamiltonian Monte Carlo with the RStan package (2.12.1). Three chains were run for each model and we assessed convergence of the model parameters by determining if the Gelman-Rubin statistic $\hat{R}$ was less than 1.05 (Gelman *et al.* 2014). We also confirmed that this statistical model could recover known transmission functions by simulating our mesocosm experiment *in silico* and testing whether the above model could both recover known parameters in ϕ and also correctly distinguish between different forms of ϕ using information criteria (see accompanying code at X).

We also tested how robust our conclusions were to the assumption that $\sigma = 1$ using two different approaches. First, we allowed this parameter to have a minimally informative half Cauchy prior with a scale parameter equal to three. This allowed for enormous variability in the dynamics of the zoospore pool. Incorporating this vague prior led to larger mean estimates of transmission from the zoospore pool (i.e. larger β_0), but also larger uncertainty around this estimate. However, the relative ranking of the different transmission models given in Table 2 in the main text did not change. The models with a dynamic zoospore pool were always better than corresponding models without the zoospore pool and the density-dependent model with a dynamic zoospore model was the best model followed by the frequency-dependent model with a zoospore pool.

Second, we explored how fixed values of σ ranging from 0.25 to 4 affected the relative rank of the models as well as the estimates of the coefficients (Figure 4, 8). Across a range of values of σ and two different measures of information criteria (WAIC and DIC), the relative rankings of the three transmission models with a dynamic zoospore pool (Table 2 in main text) stayed largely consistent, with some notable deviations between $\sigma = 1.5$ and $\sigma = 2$ (Fig. 4). We used two different information criteria as there is some question over WAIC's accuracy for time series models (Gelman *et al.* 2014). For values of $\sigma \leq 1$ the estimates of the transmission coefficients from the zoospore pool (β_0) remained relatively constant, but began increasing for $\sigma > 1$ due to the large variability in the zoospore pool dynamics (Fig. 8A). In contrast, the coefficient estimates for the density/frequency dependent transmission stayed relatively constant with a slight decreasing trend with increasing σ (Fig. 8B). Considering these sensitivity analyses, we felt that $\sigma = 1$ was a reasonable choice because 1) it did not lead to unrealistically large variability in the zoospore pool as did the uninformative prior on σ 2) it provided a conservative estimate for effect of the zoospore pool on transmission 3) the density/frequency dependent transmission coefficient β_1 was largely unaffected by the choice and 4) it resulted in model ranks that were consistent between two different information criteria and largely consistent across most values of σ that we explored.

2 R_0 for host-parasite IPMs with an environmental reservoir

R_0 for a discrete-time SIS model with an environmental reservoir

Wilber *et al.* (2016) showed how to calculate R_0 for basic host-parasite IPMs using the general

methodology developed in Klepac & Caswell (2011). This method can be extended to calculate R_0 for an IPM with an environmental reservoir. To begin, we illustrate the procedure with a simple discrete time Susceptible-Infected-Susceptible (SIS) model with a dynamic zoospore pool (Z). Take the following set of discrete dynamical equations

$$S(t+1) = S(t)s_0[1 - \phi(I(t), Z(t))] + I(t)s_I l_I \tag{6}$$

$$I(t+1) = I(t)s_I(1 - l_I) + S(t)s_0\phi(I(t), Z(t)) \tag{7}$$

$$Z(t+1) = Z(t)\nu + I(t)f \tag{8}$$

where s_0 is the survival probability for an uninfected host in a time step, s_I is the survival probability for an infected host in a time step, l_I is the probability of losing an infection in a time step, ν is the survival probability of a zoospore in a time step, f is the average number of zoospores produced by an infected individual in a time step, and $\phi(I(t), Z(t))$ is the probability of gaining an infection in a time step. Based on the results from the transmission experiment given in Table 2 in the main text, we assume that transmission depends on density-dependent host to host contact as well as transmission from the zoospore pool. Given this, we can write

$$\phi(I(t), Z(t)) = 1 - \exp[-(\beta_1 I(t) + \beta_0 Z(t))] \tag{9}$$

We can calculate R_0 for the above system of equations by rewriting them as the following matrix model

$$\begin{bmatrix} S \\ \mathbf{P} \end{bmatrix}(t+1) = \begin{bmatrix} 0 & \mathbf{0} \\ \mathbf{M}(\mathbf{P}(t)) & \mathbf{U} \end{bmatrix} \begin{bmatrix} S \\ \mathbf{P} \end{bmatrix}(t) \tag{10}$$

where the zeros simply indicate that these values do not contribute to the calculation of R_0, not that they are actually zero in the model. $\mathbf{P}(t)$ is the vector $[I(t)\ Z(t)]^T$ and $\mathbf{0}$ is a row vector [0 0]. Just focusing on the vector $\mathbf{P}$, we can write

$$\mathbf{P}(t+1) = \mathbf{M}(\mathbf{P}(t))S(t) + \mathbf{U}\mathbf{P}(t) \tag{11}$$

$\mathbf{M}(\mathbf{P}(t))$ is the vector $[s_0\phi(\mathbf{P}(t))\ 0]^T$. $\mathbf{U}$ is the 2 x 2 matrix

$$\mathbf{U} = \begin{bmatrix} s_I(1-l_I) & 0 \\ f & \nu \end{bmatrix} \tag{12}$$

To calculate R_0, we linearize $\mathbf{P}(t+1)$ about a vector $\mathbf{n}^*$. We set this vector to be a host population with only susceptibles $\mathbf{n}^* = [S^* \; \mathbf{0}]$ (Rohani *et al.* 2009; Klepac & Caswell 2011), where $\mathbf{0}$ is a vector of zeros of length $n = 2$. We then compute the Jacobian matrix evaluated at $\mathbf{n}^*$

$$\mathbf{J} = \left. \frac{d\mathbf{P}(t+1)}{d\mathbf{P}(t)} \right|_{\mathbf{n}^*} \tag{13}$$

which allows us to compute R_0 (Klepac & Caswell 2011). Computing this Jacobian requires computing $\frac{d\mathbf{M}(\mathbf{P}(t))S(t)}{d\mathbf{P}(t)}$ and $\frac{d\mathbf{U}\mathbf{P}(t)}{d\mathbf{P}(t)}$.

We immediately see that $\left. \frac{d\mathbf{U}\mathbf{P}(t)}{d\mathbf{P}(t)} \right|_{\mathbf{n}^*} = \mathbf{U}$. $\left. \frac{d\mathbf{M}(\mathbf{P}(t))S(t)}{d\mathbf{P}(t)} \right|_{\mathbf{n}^*}$ requires application of the chain rule for differentiation and we see that

$$\left. \frac{d\mathbf{M}(\mathbf{P}(t))S(t)}{d\mathbf{P}(t)} \right|_{\mathbf{n}^*} = \mathbf{M}^* = \begin{bmatrix} s_0 S^* \beta_1 & s_0 S^* \beta_0 \\ 0 & 0 \end{bmatrix} \tag{14}$$

R_0 is given by (Klepac & Caswell 2011)

$$R_0 = \max \text{eig}(\mathbf{M}^*(\mathbb{1} - \mathbf{U})^{-1}) \tag{15}$$

and plugging into $\mathbf{M}^*$ and $\mathbf{U}$ given above we get

$$R_0 = \frac{s_0 S^* \beta_1}{1 - s_I(1-l_I)} + \frac{s_0 S^* \beta_0 f}{(1-\nu)[1 - s_I(1-l_I)]} \tag{16}$$

Similar to the continuous time result given in Rohani *et al.* (2009), we see that R_0 is a combination of both transmission from the hosts (first term) and the environment (second term). Setting $\beta_0 = 0$, we recover the simple SIS R_0 given in Wilber *et al.* (2016) and Oli *et al.* (2006).

R_0 for the host parasite IPM with an environmental reservoir

To generalize this to a host-parasite IPM model with an environmental reservoir where the I class is now potentially infinitely many classes, we can take the following steps. First, we recognize that in practice IPMs are analyzed using the mid-point rule (Easterling *et al.* 2000) such that there are a finite number of I classes, namely n classes. Therefore, we can think of our IPM as a generalization of the SISZ model presented above such that $\mathbf{P}(t)$ is a vector of length $n+1$,

$\mathbf{M}(\mathbf{P}(t))$ is now a vector of length $(n+1)$ and $\mathbf{U}$ is a $(n+1)$ x $(n+1)$ matrix. The plus one is because the environmental reservoir Z is part of the $\mathbf{P}$ vector.

For the first n x n elements in $\mathbf{U}$, the element in the ith row and the jth column is given by

$$u_{ij} = s(x_j)(1 - l(x_j))G(x_i, x_j)\Delta \tag{17}$$

which gives the probability of an individual in the jth load class with parasite load x_j, surviving $(s(x_j))$, not losing its infection $(1 - l(x_j))$, and transitioning to the load class of x_i in a time step $(G(x_i, x_j))$. Δ is a result of using the midpoint rule to discretize the continuous IPM and is used to convert the probability density $G(x_i, x_j)$ into a probability (e.g. see Easterling *et al.* 2000; Wilber *et al.* 2016). The $n+1$th row of $\mathbf{U}$ is the vector $[f_x\mathbf{x} \;\; \nu]$ of length $n+1$, where we assume that an infected host in class j produces an average of $f_x x_j$ parasites in a time step into the zoospore pool. $\mathbf{x}$ is a vector of length n that contains the corresponding parasite loads for the n infected classes. The $n+1$th column of $\mathbf{U}$ is the vector $[\mathbf{0} \;\; \nu]^T$, where $\mathbf{0}$ is of length n.

$\mathbf{M}(\mathbf{P}(t))$ is given by a vector of length $n+1$ where the first $i = 1, \ldots, i, \ldots n$ elements are given by

$$m_i = s_0\phi(\boldsymbol{\beta}^T\mathbf{I}(t))G_0(x_i)\Delta \tag{18}$$

where $\boldsymbol{\beta}^T$ is a vector of length $n+1$ with the first n elements being β_1 and the $n+1$th element being β_0. $\left.\frac{d\mathbf{M}(\mathbf{P}(t))S(t)}{d\mathbf{P}(t)}\right|_{\mathbf{n}^*} = \mathbf{M}^*$ is given by a $(n+1)$ x $(n+1)$ matrix where the first n columns are given by $[s_0S^*\beta_1G_0(\mathbf{x})\Delta \quad 0]^T$ and the $n+1$th column is given by $[s_0S^*\beta_0G_0(\mathbf{x})\Delta \quad 0]^T$. $G_0(\mathbf{x})$ indicates that the function $G_0(x)$ is evaluated at each element in $\mathbf{x}$, resulting in a vector of length n.

Given $\mathbf{M}^*$ and $\mathbf{U}$ we can again calculate R_0 as (Klepac & Caswell 2011)

$$R_0 = \max \text{ eig}(\mathbf{M}^*(\mathbb{1} - \mathbf{U})^{-1}) \tag{19}$$

In the main text, we use this formulation to numerically calculate R_0 for the *R. muscosa*-Bd IPM model with and without an environmental reservoir.

3 The hybrid model

3.1 Within-year component of the hybrid model

The model described by equations 6-8 in the main text may be sufficient to describe the dynamics of an initial epizootic, but in order to examine Bd-induced extinction dynamics in *R. muscosa* populations a number of additions need to be made. First, the tadpole stage of *R. muscosa* has been shown to play an important role in generating enzootic dynamics in *R. muscosa* populations (Briggs *et al.* 2005, 2010). *R. muscosa* can spend three years as tadpoles and thus we include three additional tadpole stages into the model T_1, T_2, and T_3 (Briggs *et al.* 2005). Considering equations 6-8, we can add this tadpole class and update our zoospore pool equation as follows

$$T_i(t+1) = T_i(t)s_{T_i} \tag{20}$$

$$Z(t+1) = Z(t)\nu + \sum_{i=1}^{3} \mu_{T_i} T_i(t) + \mu_A \int_{L_x}^{U_x} \exp(x) I_A(x,t)dx - \psi(S_A(t), Z(t)) \tag{21}$$

The equation $T_i(t+1)$ describes how the number of tadpoles in class i changes from time t to time $t+1$. We do not explicitly model the fungal load on tadpoles. Instead, we assume all tadpoles are immediately infected with Bd and have a constant contribution to the zoospore pool. This is justified by the observation that most tadpoles in *R. muscosa* populations carry high fungal loads, even in enzootic populations (Briggs *et al.* 2010). *R. muscosa* tadpole survival is not affected by Bd infection. Therefore, the within-season dynamics of T_i are simply given by the probability of a tadpole surviving from time t to $t+1$, which is s_{T_i}. Notice that infected tadpoles are now also contributing μ_{T_i} zoospores to the zoospore pool at each time step. Previous models of this system have included a subadult stage after metamorphosis that can last 1-2 years (Briggs *et al.* 2005, 2010). For simplicity, we are ignoring it here.

R. muscosa populations also experience seasonal temperature fluctuations in which lake temperatures drop to approximately 4 °C in the winter (in the unfrozen portion of a lake where the frogs overwinter) and reach approximately 20 °C in the summer (Knapp *et al.* 2011). We account for this seasonal variability by imposing a deterministically fluctuating environment on the *R. muscosa*-Bd IPM. We assumed that temperature follows a sinusoidal curve with a period of 1 year and a minimum temperature of 4 °C and a maximum temperature of 20 °C (Fig. 1A). At each discrete time point within a season, a new temperature is calculated based on the sinusoidal curve and the temperature-dependent vital rate functions in equations 6-10

are updated accordingly (see Table 1 in the main text and Appendix Fig. 1 for temperature-dependent vital-rate functions).

3.2 Between-year component of the hybrid model

In the within-year component of the hybrid model a time step is 3 days. This time step is on the same scale as Bd dynamics. However, *R. muscosa* demography occurs on a slower scale. We assume that *R. muscosa* demographic dynamics occur on a yearly time scale (Briggs *et al.* 2005), such that once a year tadpoles either age a year or metamorphose and adults reproduce. The mortality for each stage as well as all disease dynamics are accounted for in the within-year component of the IPM, thus the between-year component only includes the following demographic events (Fig. 1C in the main text)

$$T_1(t+1) = p_A \lambda_0 S_A(t) + p_A \int_{L_x}^{U_x} \lambda(x) I(x,t) dx \tag{22}$$

$$T_2(t+1) = p_{T_1} T_1(t) \tag{23}$$

$$T_3(t+1) = p_{T_2} T_2(t) \tag{24}$$

$$S_A(t+1) = [(1-p_{T_1}) m_{T_1} T_1(t) + (1-p_{T_2}) m_{T_2} T_2(t) + m_{T_3} T_3(t)] \exp(-A(t)/K) \tag{25}$$

$$I_A(x', t+1) = I_A(x', t) \tag{26}$$

$$Z(t+1) = Z(t) \tag{27}$$

where these events only occur once per year (Fig. 1 in the main text). When these demographic events occur each year, they occur after the disease dynamics defined above, but in the same time step from t to $t+1$. Equation 21 gives the contribution of adult frogs to the T_1 tadpole class. p_A defines the probability of an adult reproducing, λ_0 is the mean reproductive output of uninfected adults and $\lambda(x)$ is the mean reproductive output of an adult with a Bd load of x. Equation 22 gives the probability of a T_1 tadpole not metamorphosing (p_{T_1}) and transitioning to a T_2 tadpole. Equation 23 describes the changes in the T_3 class via the probability of a T_2 tadpole not metamorphosing (p_{T_2}) and transitioning to a T_3 tadpole. Equation 24 describes T_1, T_2 and T_3 tadpoles metamorphosing, surviving metamorphosis, and recruiting as uninfected adults. Recruitment of tadpoles to the adult stage is a density-dependent process following a Ricker function with adult density ($A(t)$) and a parameter that is proportional to the carrying capacity (K) (Briggs *et al.* 2005). Because we have no empirical evidence for Bd-induced fertility reduction

in *R. muscosa*, we assumed that reproduction in uninfected adults was the same as reproduction in infected adults. We also assume that tadpoles lose their infection during Bd metamorphosis (Briggs *et al.* 2010). Finally, equations 25 and 26 indicate that infected individuals ($I_A(x', t+1)$) and the zoospore pool ($Z(t+1)$) do not change during the demographic update.

4 Converting the hybrid model into an individual-based model with demographic stochasticity

The simplest way to include demographic stochasticity into the hybrid model is to assume that demographic stochasticity is given by sampling error and allow all demographic transitions to occur following some probability distribution (Caswell 2001; Schreiber & Ross 2016). To illustrate this, recall that to analyze the hybrid Integral Projection Model we discretized the continuous class $\int_a^b I(x,t)dx$ (which gives the number of frogs with a ln *Bd* load between a and b at time t) into 30 load classes using the midpoint rule (Easterling *et al.* 2000). We can now loosely think about our hybrid model as a matrix model with 3 tadpole + 1 susceptible adult + 30 infected adult + 1 zoospore pool = 35 stages. Let's call the transition matrix $\mathbf{A}$. Following Caswell (2001) and Schreiber & Ross (2016), we can decompose our hybrid model into components for infection dynamics (i.e. growth, loss, initial infection gain), host survival, disease transmission, and demographic transitions ($\mathbf{T}$) and reproduction ($\mathbf{F}$) such that $\mathbf{A} = \mathbf{T} + \mathbf{F}$. The matrix $\mathbf{T}$ gives the probabilities of an individual in stage j transitioning to stage i in a 3 day time step. However, $\mathbf{T}$ is not a stochastic matrix (i.e. the columns do not sum to one) because individuals in each stage also have a survival probability and one potential transition during each time step is to a "dead" class. We can augment this matrix $\mathbf{T}$ with an extra row $\mathbf{d}$ specifying the "dead" class where each entry in this row can be defined as $d_{36,j} = 1 - \text{sum}(\mathbf{T}_{,j})$. $\text{sum}(\mathbf{T}_{,j})$ gives the sum of the jth column of the $\mathbf{T}$ matrix. The new augmented matrix $\mathbf{T}^*$ is fully stochastic (Caswell 2001; Schreiber & Ross 2016). Assuming each individual transitions independently of each other, for each time step t the transition of a single individual in class j to another class i (including the "dead" class) follows a multinomial distribution with a probability vector $\mathbf{p_j}$ given by the jth column of $\mathbf{T}^*$: $\mathbf{p_j} = \mathbf{T}^*_{,\mathbf{j}}$. At any time step we could simulate what happens to n individuals in class j by drawing from a multinomial distribution with the total number of trials equal to n and the probability vector equal to $\mathbf{p_j}$. The resulting random vector would be of length 36 specifying the stages that the n individuals of stage j at time t now occupy at time $t+1$ (including death).

In addition to individual transitions (or "births"), we also need to account for the births defined in the **F** matrix. In the hybrid model, there are two types of births we account for in the **F** matrix: the production of T_1 tadpoles from adults (infected and uninfected) and the production of zoospores from tadpoles and infected adults. As is, the fecundity matrix **F** only specifies the mean production of T_1 tadpoles and zoospores. To make this probabilistic, we need to specify a distribution around this mean. We assumed that the production of tadpoles followed a Poisson distribution with mean $A(t)p_A\lambda$, where $A(t) = S_A(t) + \int_{L_x}^{U_x} I_A(x,t)dx$ is the number of adults in the population at time t, p_A is the probability of an adult reproducing and λ is the mean number of tadpoles produced. We also assumed that the number of zoospores shed into the zoospore pool from tadpoles and adults at each time step followed a Poisson distribution with mean $\sum_{i=1}^{3} \mu_{T_i} T_i(t) + \mu_A \int_{L_x}^{U_x} \exp(x) I_A(x,t)dx$. With this distributional assumption, we can then easily calculate the contribution of T_1 tadpoles and zoospores over a time step t as a draw from a Poisson distribution with a mean given by the appropriate entry in the **F** matrix. Combining these draws from a Poisson distribution with the draws from the multinomial distribution described above, we can simulate the individual-based representation of our hybrid model with any density-dependent assumptions about recruitment or disease transmission in addition to any assumptions about temperature-dependent vital rates. This can be done by updating the various transition probabilities using the appropriate densities or temperatures at each time step and performing the previously described stochastic draws with the updated transition probabilities. See the function `multiseason_stochastic_simulation` for the R code necessary to implement this stochastic simulation.

References

Briggs, C. J., Knapp, R. A. & Vredenburg, V. T. (2010). Enzootic and epizootic dynamics of the chytrid fungal pathogen of amphibians. *Proceedings of the National Academy of Sciences of the United States of America*, 107, 9695–9700.

Briggs, C. J., Vredenburg, V. T., Knapp, R. A. & Rachowicz, L. J. (2005). Investigating the population-level effects of chytridiomycosis: an emerging infectious disease of amphibians. *Ecology*, 86, 3149–3159.

Caswell, H. (2001). *Matrix Population Models: Construction, Analysis, and Interpretation*. 2nd edn. Sinauer, Sunderland, Massachusetts.

Easterling, M. R., Ellner, S. P. & Dixon, P. M. (2000). Size-specific sensitivity: applying a new structured population model. *Ecology*, 81, 694–708.

Gelman, A., Carlin, J. B., Stern, H. S., Dunson, D. B., Vehtari, A. & Rubin, D. B. (2014). *Bayesian Data Analysis*. 3rd edn. Taylor & Francis Group, LLC, Boca Raton.

Klepac, P. & Caswell, H. (2011). The stage-structured epidemic: Linking disease and demography with a multi-state matrix approach model. *Theoretical Ecology*, 4, 301–319.

Knapp, R. A., Briggs, C. J., Smith, T. C. & Maurer, J. R. (2011). Nowhere to hide: impact of a temperature-sensitive amphibian pathogen along an elevation gradient in the temperate zone. *Ecosphere*, 2, art93.

Oli, M. K., Venkataraman, M., Klein, P. A., Wendland, L. D. & Brown, M. B. (2006). Population dynamics of infectious diseases: A discrete time model. *Ecological Modelling*, 198, 183–194.

Rohani, P., Breban, R., Stallknecht, D. E. & Drake, J. M. (2009). Environmental transmission of low pathogenicity avian influenza viruses and its implications for pathogen invasion. *Proceedings of the National Academy of Sciences*, 106, 10365–10369.

Schreiber, S. J. & Ross, N. (2016). Individual-based integral projection models: the role of size-structure on extinction risk and establishment success. *Methods in Ecology and Evolution*, 7, 867–874.

Wilber, M. Q., Langwig, K. E., Kilpatrick, A. M., Mccallum, H. I. & Briggs, C. J. (2016). Integral Projection Models for host-parasite systems with an application to amphibian chytrid fungus. *Methods in Ecology and Evolution*, 7, 1182–1194.

Woodhams, D. C., Alford, R. A., Briggs, C. J., Johnson, M. & Rollins-Smith, L. A. (2008). Life-history trade-offs influence disease in changing climates: Strategies of an amphibian pathogen. *Ecology*, 89, 1627–1639.

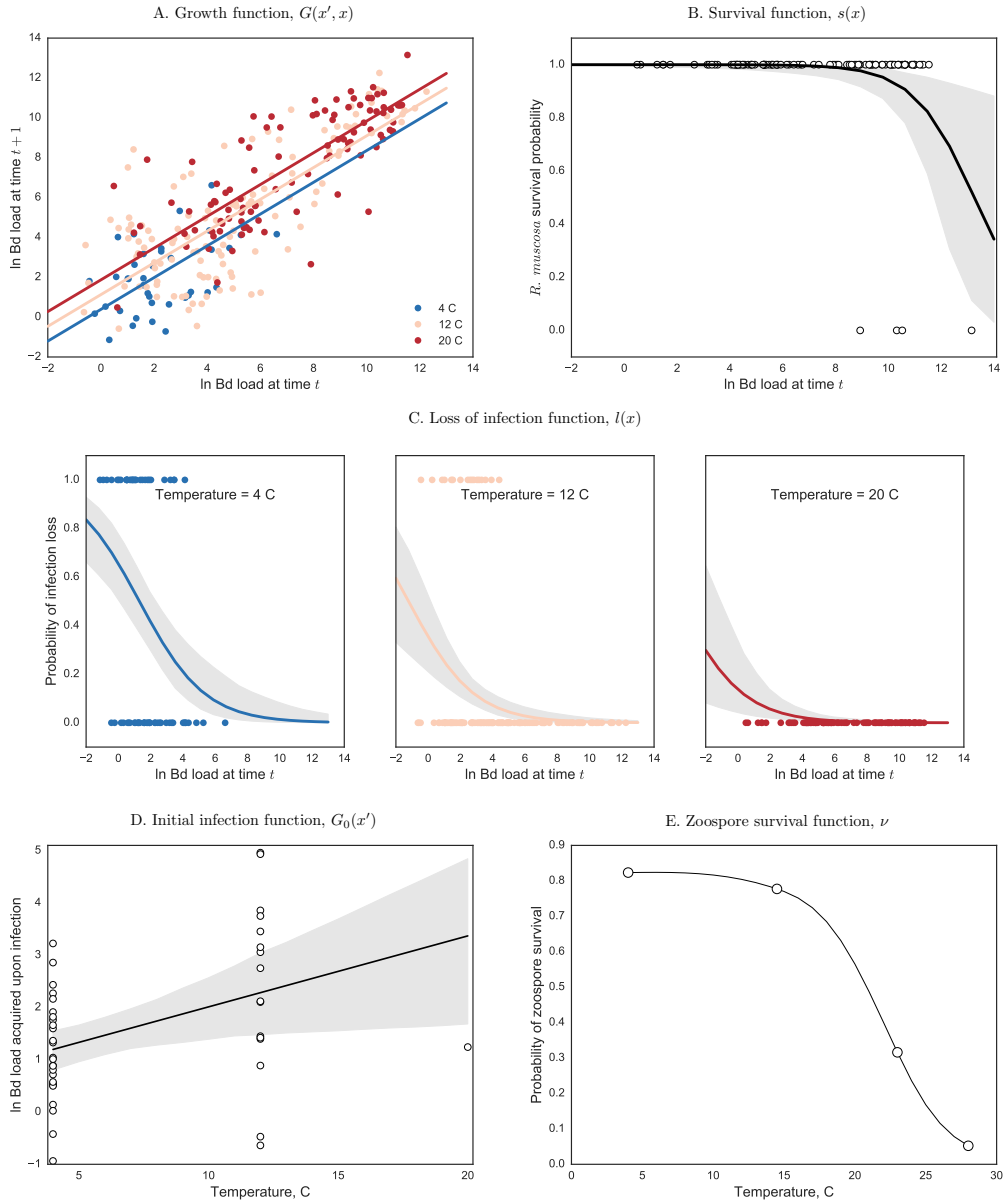

Figure 1: The various vital rate functions estimated from laboratory data given in Wilber *et al.* (2016) and Woodhams *et al.* (2008). In all plots, points give the laboratory data, lines give the model fit, and gray regions given the 95% credible interval about the predictions. **A.** The temperature-dependent growth function $G(x', x)$ where temperature is included as a continuous covariate in the growth function. 95% CIs where not included for visual clarity. **B.** The survival function $s(x)$ which dictates the probability of an adult *R. muscosa* surviving with a given load over a three day time step. **C.** The loss of infection function $l(x)$ which gives the load- and temperature-dependent probability of an adult *R. muscosa* losing a *Bd* infection over a three day time step. **D.** The initial infection function $G_0(x')$ that specifies the temperature-dependent probability density of gaining an initial infection of size x'. **E.** The zoospore survival function ν that gives the temperature-dependent probability of a zoospore surviving over three days as given in Woodhams *et al.* (2008). No uncertainty was included around this prediction.

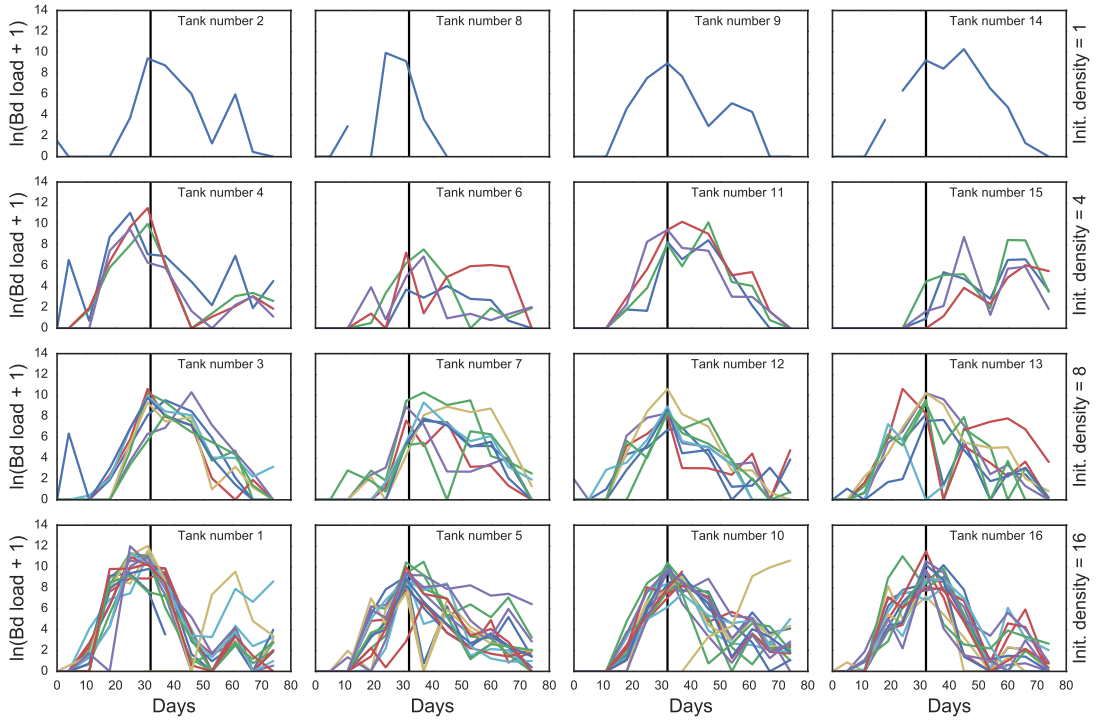

Figure 2: The observed *Bd* load trajectories for individual frogs in the density-dependent mesocosm experiment described in the main text. Tanks/mesocosms had an initial density of either 1, 4, 8, or 16 frogs and were assigned numbers 1 - 16 as indicated on a panel. The different colored lines are the different *Bd* load trajectories for the frogs in given tank. The black vertical line indicates day 32 of the experiment, after which there was an unexplained decrease in zoospore load in the infected frogs in all mesocosms in which frogs were infected by this time point. The consistency of the decline between treatments, between mesocosms, and between frogs suggests the involvement of an external environmental driver or a frog immune response. Data after this time point was not used when fitting the transmission models described in the main text.

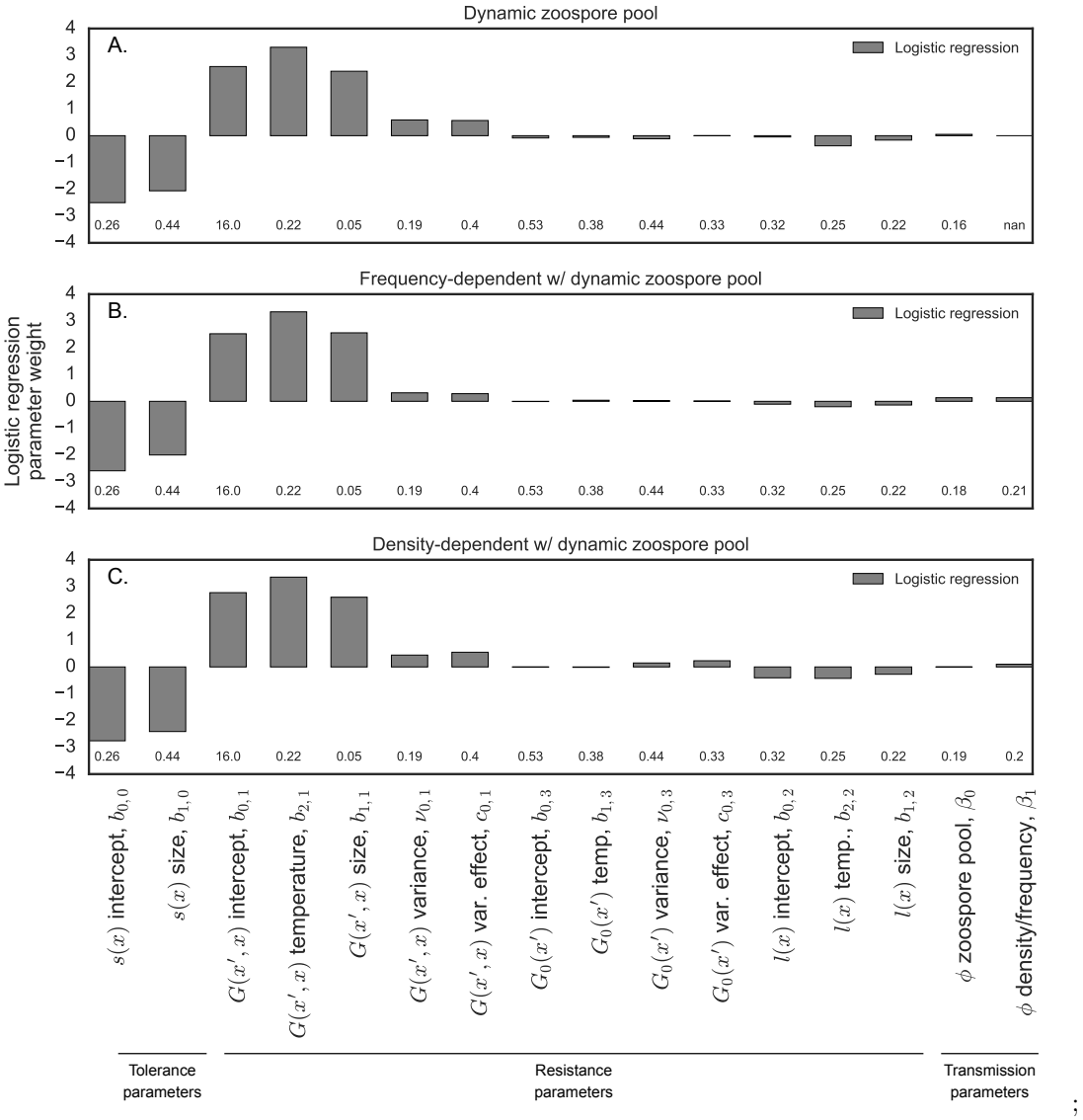

;

Figure 3: The results of the global sensitivity analysis similar to Figure 4 in the main text. However, instead of perturbing parameters by drawing from a lognormal distribution with median 1 and $\sigma = 0.3$, we drew the parameters from their corresponding posterior distribution from the fitted bayesian models on the temperature and transmission experiments described in the main text. This allowed for correlation between the parameters as well as allowing some parameters to have larger variability than others, strictly based on the variability in the posterior distribution. The above plot gives the standardized coefficients from a regularized logistic regression. The height of a bar indicates how sensitive extinction risk was to this parameter. The direction indicates whether increasing the parameter increased or decreased the probability of extinction. The values under each bar give the coefficient of variance (CV) for each parameter, calculated from that parameter's posterior distribution. The results from this sensitivity analysis were qualitatively consistent with the approach used in the main text: disease-induced extinction was far more sensitive to the parameters in the growth function ($G(x', x)$) (resistance) and the survival function (tolerance) than to parameters in the transmission function. Pruned regression trees also confirmed the important interaction between the growth function and the survival function.

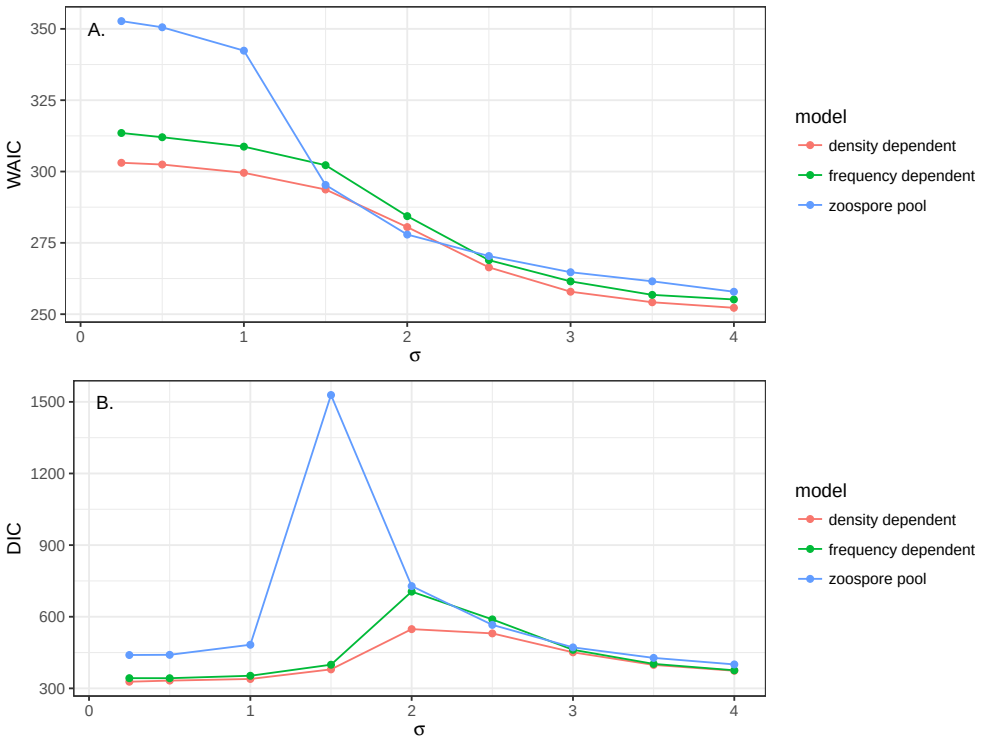

Figure 4: Comparing two information criteria when fitting the latent zoospore model to the mesocosm transmission experiment with different levels of process error in the latent zoospore pool (given by σ). The above plots show WAIC (**A.**) and DIC (**B.**) values for three different transmission models fit to the experimental data: density-dependent transmission with a dynamic zoospore pool (pink), frequency-dependent transmission with a dynamic zoospore pool (green), and only dynamic zoospore pool (blue). When $\sigma \leq 1$ and $\sigma \geq 2.5$, the relative model rankings are consistent for both WAIC and DIC. However, between 1 and 2.5 the information criteria for the dynamic zoospore pool transmission function either drastically decreases (WAIC) or drastically increases (DIC).

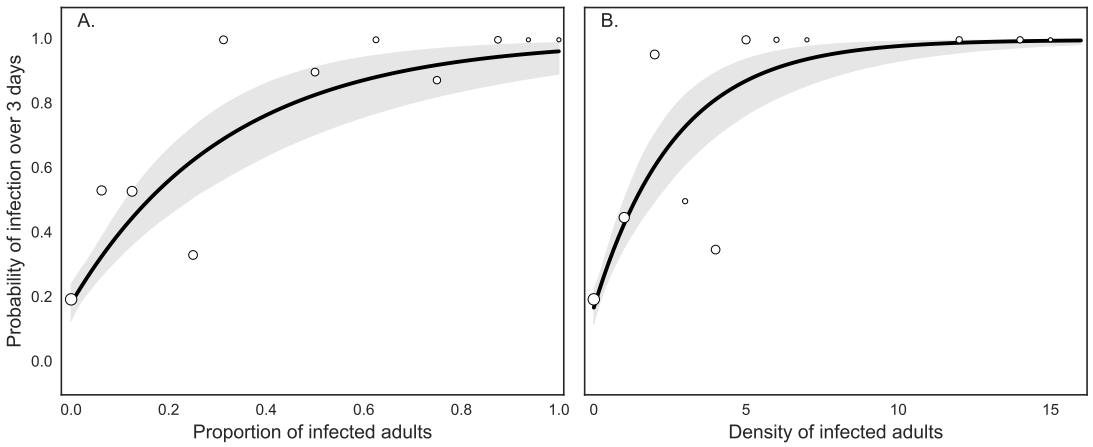

Figure 5: Predictions from the best fit frequency-dependent and density-dependent transmission functions with a dynamic zoospore pool, as estimated from the mesocosm experiment described in the main text. Because the data used to fit these transmission models is Bernoulli (0 or 1) and there are three dimensions of predictor variables (time, host density/frequency, and zoospore density) it is difficult to give a visual representation of model fit. Here we show the marginal predictions (black lines) from the frequency-dependent and density-dependent transmission models, fixing the time step at 3 days and the zoospore pool at 1096 zoospores. The gray region gives the 95% credible interval around these predictions. The open circles give the observed proportion of frogs that transitioned from uninfected to infected with the proportion/density of infected individuals given on the x-axis (pooled across different time steps and zoospore pool sizes). The size of the points indicates the sample size of each point, with larger points indicating larger sample size ($n = 333$ total samples distributed among the points). **A.** The predictions from the best-fit frequency-dependent transmission function ($\phi = 1 - \exp\left(-(\beta_0 \ln(Z+1) + \beta_1 \frac{I}{A})\Delta t\right)$) **B.** The predictions from the best-fit density-dependent transmission function ($\phi = 1 - \exp\left(-(\beta_0 \ln(Z+1) + \beta_1 I)\Delta t\right)$)

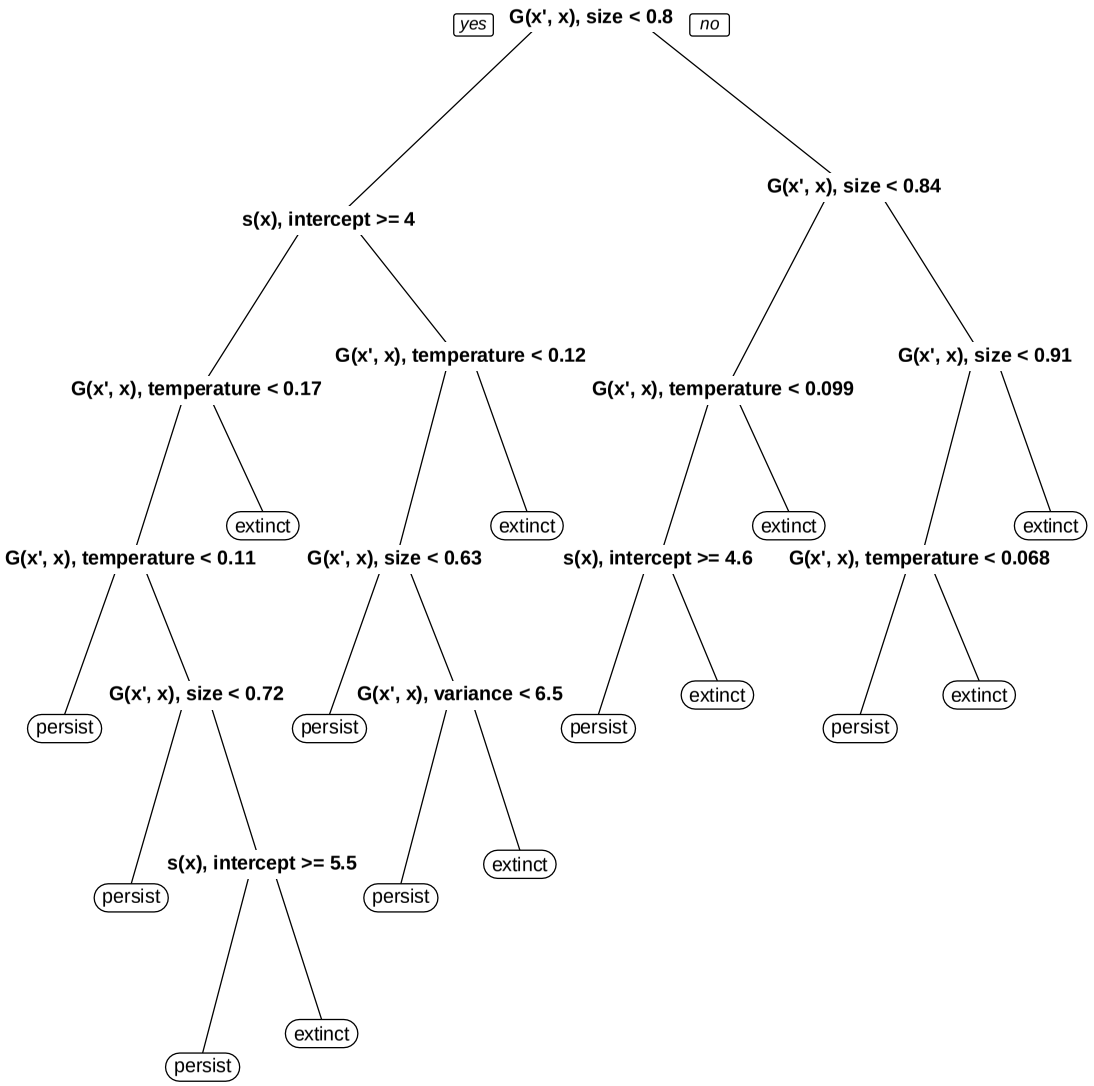

Figure 6: A. The pruned regression tree for the model with density-dependent transmission with a dynamic zoospore pool. Shows a visual representation of how the various transmission, resistance, and tolerance parameters interacted to affect *Bd*-induced host extinction. In particular, parameters of the growth function determining host resistance ($G(x', x)$) and the survival function determining host tolerance ($s(x)$) interact to predict extinction or persistence.

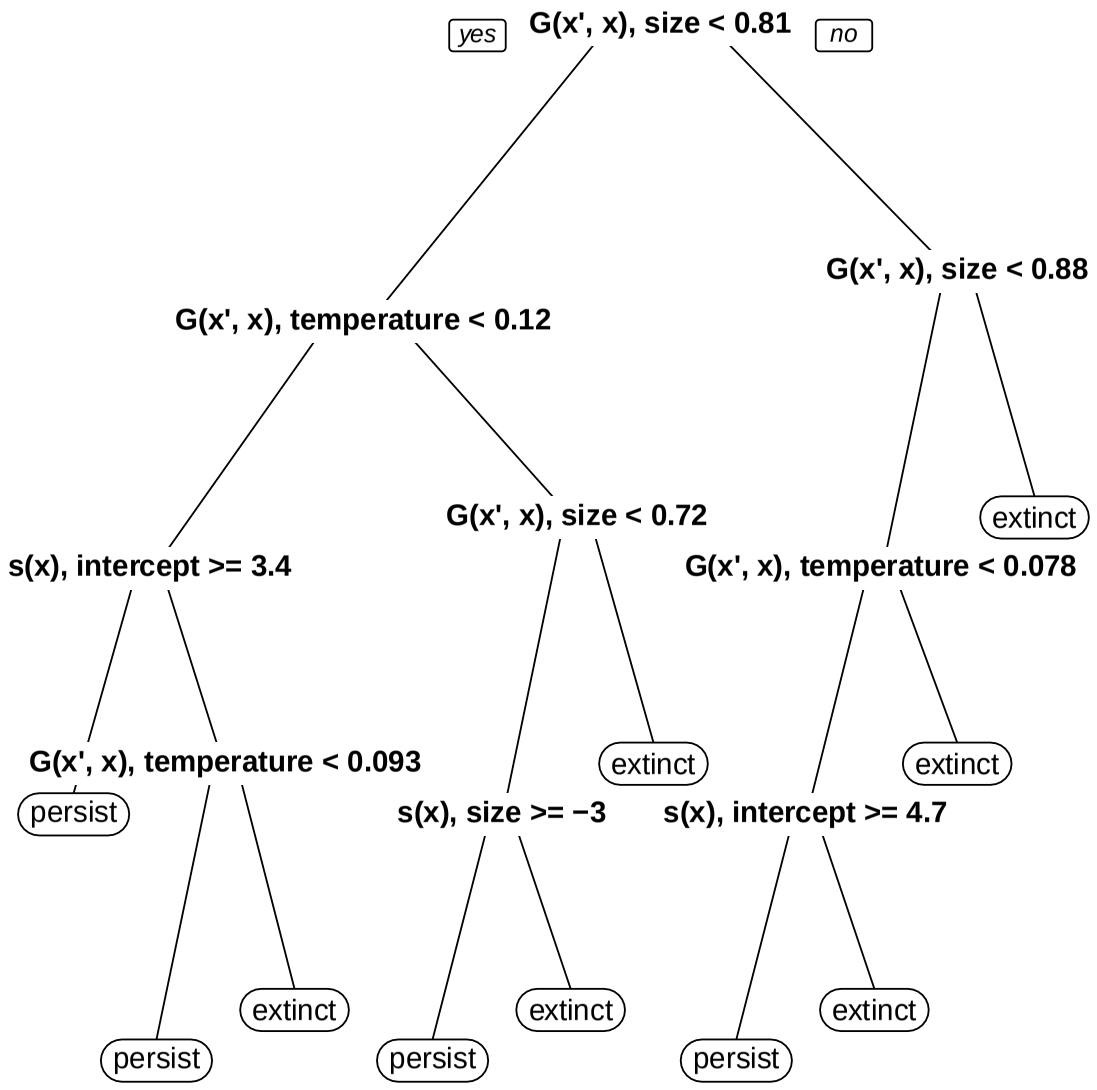

Figure 6B. The pruned regression tree for the model with frequency-dependent transmission with a dynamic zoospore pool. Shows a visual representation of how the various transmission, resistance, and tolerance parameters interacted to affect *Bd*-induced host extinction. In particular, parameters of the growth function determining host resistance ($G(x', x)$) and the survival function determining host tolerance ($s(x)$) interact to predict extinction or persistence.

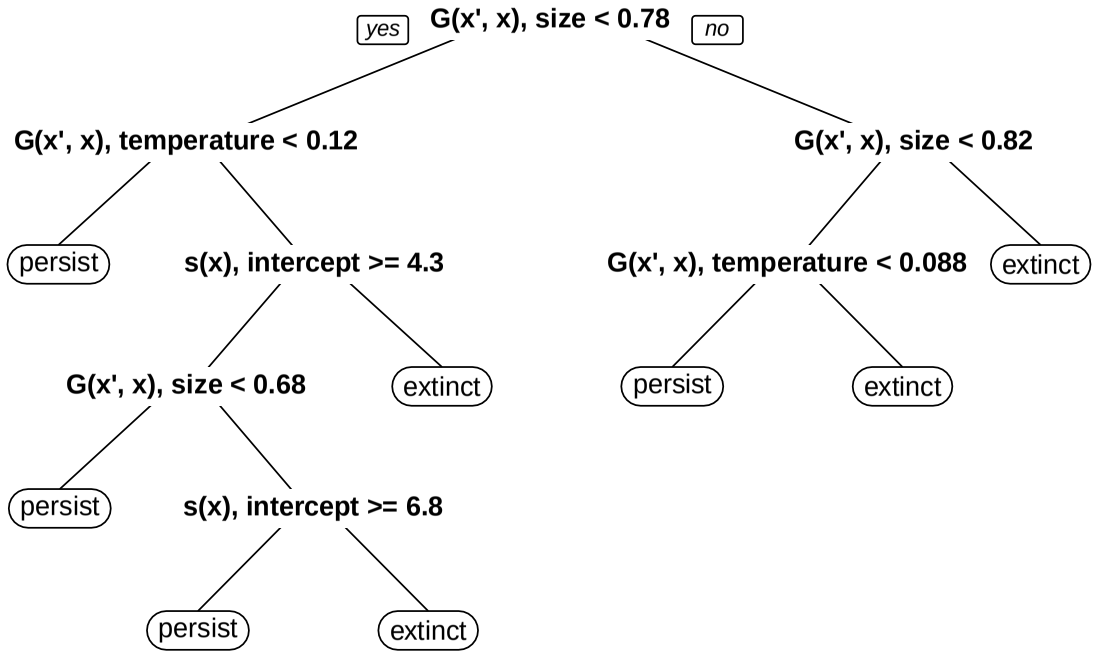

Figure 6C. The pruned regression tree for the model with transmission from a dynamic zoospore pool. Shows a visual representation of how the various transmission, resistance, and tolerance parameters interacted to affect *Bd*-induced host extinction. In particular, parameters of the growth function determining host resistance ($G(x', x)$) and the survival function determining host tolerance ($s(x)$) interact to predict extinction or persistence.

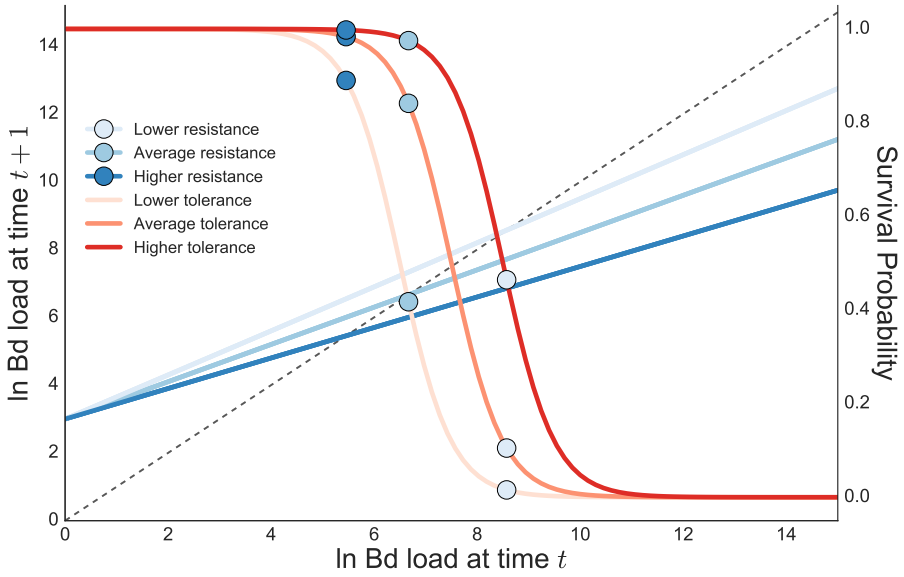

Figure 7: The interaction between the growth function determining host resistance (blue lines) and the survival function determining host tolerance (red lines) has large impacts on host survival probability. The solid blue lines of different shades give three different growth functions that describe how Bd load changes from time step t to time step $t+1$. The growth functions have different slopes representing different levels of resistance. When one of the growth functions crosses the dashed 1:1 line, this indicates that the Bd load at time t will be the same as the Bd load at time $t+1$ (i.e. stasis). The red lines of different colors specify different survival functions with different levels of tolerance. The corresponding blue colored circle on one of the red survival curves gives the probability of a host surviving a time step with the given Bd load at stasis. Each red survival curve has three different blue dots for each of the three growth functions. Because of the strong non-linearity of the survival function, changes in the Bd load at stasis can lead to disproportionate changes in survival probability. However, the direction and magnitude of these changes depends on the degree of tolerance represented in the survival curve.

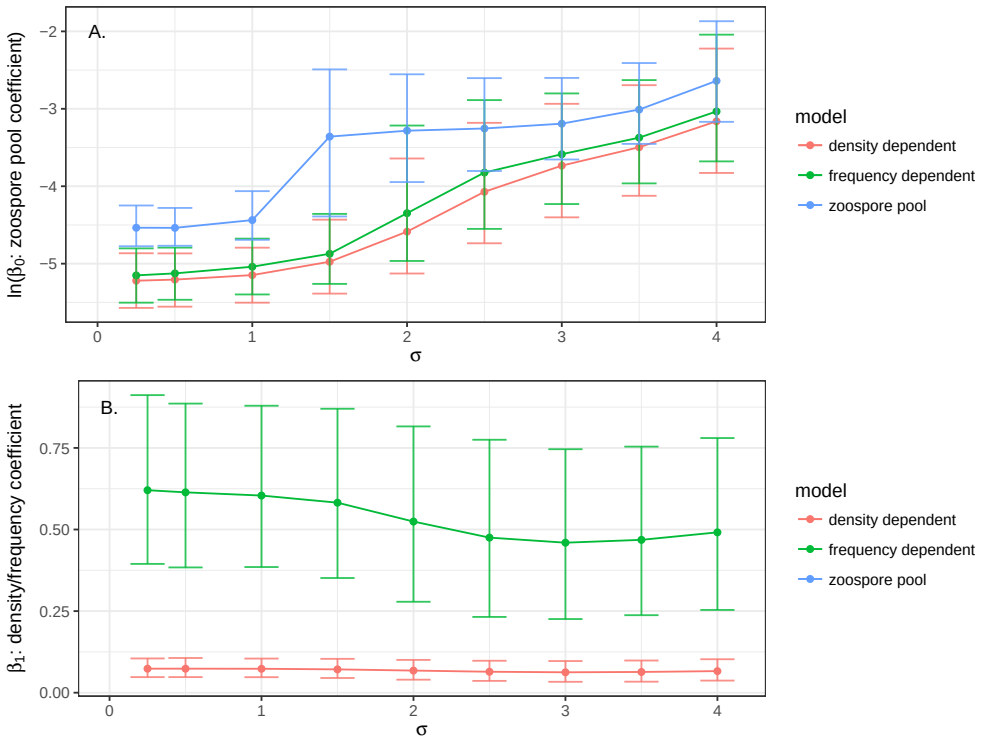

Figure 8: Comparing the estimates of the transmission coefficients (β_0: the zoospore pool coefficient, β_1: the density/frequency dependent coefficient) when fitting the latent zoospore model to the mesocosm transmission experiment with different levels of process error (given by σ). **A.** The zoospore pool coefficient shows a marked increase after $\sigma = 1$. This is driven by the large variability in the trajectory of the zoospore pool, such the transmission coefficient needs to increase in order to contribute to transmission when, by chance, the zoospore pool may crash to very low levels under the high σ/process error scenarios. **B.** In contrast, the transmission coefficient β_1 determining density or frequency-dependent host contacts are relatively consistent across σ, with a slight decreasing trend. These is no blue line in B. because the transmission model with only a dynamic zoospore pool does not have a coefficient β_1. The error bars are 95% credible intervals around the coefficient estimates.